IEEE Access
Multidisciplinary | Rapid Review | Open Access Journal

Received August 1, 2019, accepted August 15, 2019, date of publication August 26, 2019, date of current version September 9, 2019.

Digital Object Identifier 10.1109/ACCESS.2019.2937395

Impedance-Based Oscillatory Stability Analysis of High Power Electronics-Penetrated Power Systems–A Survey

YONG HU[1], SIQI BU[1], (Senior Member, IEEE), BIN ZHOU[2], (Senior Member, IEEE), YI LIU[3], AND CHENG-WEI FEI[4]

[1]Department of Electrical Engineering, The Hong Kong Polytechnic University, Hong Kong
[2]College of Electrical and Information Engineering, Hunan University, Changsha 410082, China
[3]Institute of Electrical Engineering, Chinese Academy of Sciences, Beijing 100190, China
[4]Department of Aeronautics and Astronautics, Fudan University, Shanghai 200433, China

Corresponding author: Siqi Bu (siqi.bu@polyu.edu.hk)

This work was supported in part by the Department of Electrical Engineering, The Hong Kong Polytechnic University, through the Start-up Fund Research Project, under Grant 1-ZE68, in part by the Hong Kong Research Grant Council for the Research Projects under Grant 25203917, Grant 15200418, and Grant 15219619, and in part by the National Natural Science Foundation of China for the Research Project under Grant 51807171.

ABSTRACT With increasing power electronics integrated into the power grids, the new types of oscillation issues have posed a critical threat to the secure operation of power grids. Apart from the conventional eigenvalue-based analysis, the impedance-based analysis becomes more attractive for the assessment of the oscillatory stability. This paper presents a systematic survey on the technical matters of the emerging impedance-based oscillatory stability analysis of power systems with high power electronics penetration. Firstly, the detailed derivation of impedance models of the power electronic converter-connected equipment are discussed. Then, common coordinate systems for the derivation of impedance models, as well as the characteristics of the impedance model in different coordinate systems are surveyed. On this basis, the aggregation of the individual impedance models is introduced to derive the lumped impedance model. Additionally, two typical impedance-based oscillatory stability criteria are demonstrated and discussed in details. Finally, the advantages as well as the limitations of the impedance-based oscillatory stability analysis, and the contributions as well as the challenges of the existing studies are summarized. A list of relevant literature is accommodated in the end.

INDEX TERMS Oscillatory stability, impedance-based analysis, derivation of impedance models, lumped impedance model, stability criteria.

I. INTRODUCTION

A. BACKGROUND

Energy depletion and environmental problems boost the development of renewable energy generations [1], among which wind and photovoltaic (PV) power generations are the most representative. Unlike conventional generation units, the power electronic converters are indispensable for the integration of renewable energy generations to the power grid [2], [3]. In addition, the development of new transmission technologies, such as flexible AC transmission systems (FACTS) and high-voltage DC (HVDC) systems, also lead to the consequence that the conventional power equipment (e.g., transmission lines, transformers, series compensation equipment) has to coexist with the large number of power electronic converters [4], [5]. The current status of the power grid with multiple emerging technologies can be illustrated by Figure 1. In some optimization-related studies of the local distribution network, the external power grid is usually seen as an ''ideal infinite power source'' (e.g., the research in [6] and [7]). However, big amount of power electronics has brought complex non-linearity and dynamics to the power grid [8], [9]; the external power grid can no longer be regarded as the ''ideal infinite power source'', but the ''weak grid'' [10]. As an important aspect of power system dynamics, the oscillation issue has been significantly

The associate editor coordinating the review of this article and approving it for publication was Yang Li.

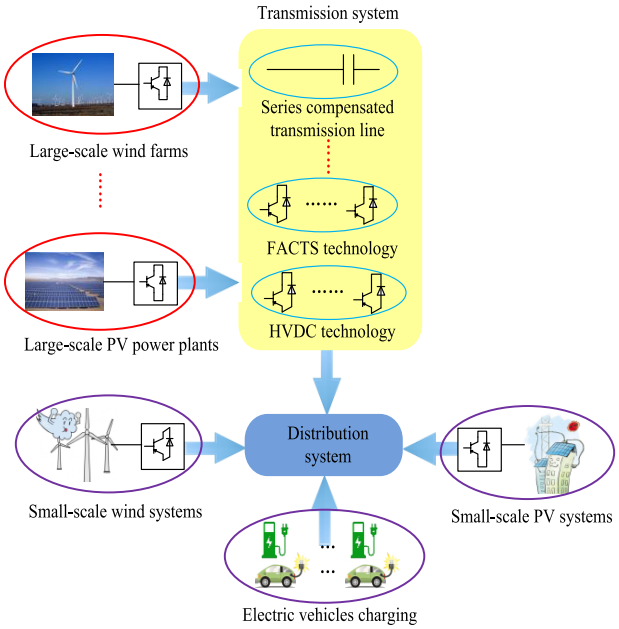

FIGURE 1. Current status of power grids with emerging technologies.

impacted [11]. The aforementioned multiple emerging technologies inevitably bring potential risks to the overall stability of power systems, as well as the secure operation of local power grids [12], [13].

B. OSCILLATION ISSUES AND ANALYSIS METHODS

Since each power electronic device brings complex dynamics in some frequency ranges, they have a great potential to generate various types of interactions with each other, which brings the emerging forms of the oscillation [14]. On the other hand, with the number of power electronic converters becomes huge, it is more difficult to identify which power electronics in the system is the main source of the oscillation, which further complicates the oscillation assessment. In the existing literature related to oscillation issues, the sub-synchronous oscillation/resonance (SSO/SSR) and the low-frequency oscillation (LFO) have attracted the major attention of researchers.

An SSO/SSR incident caused by the interactions between the type-3 wind turbines and the series compensation equipment happened in Texas in 2009, which has led to the damage to system devices and motivated the research on the SSO/SSR issues caused by the power electronics [15], [16]. Shortly after this accident, the authors in [17] put forward the dynamic model of the type-3 wind turbines for the SSO/SSR analysis. In recent few years, more SSO/SSR phenomena have been observed in the power systems with growing number of power electronics, such as the SSO/SSR occurring in Guyuan, Hebei Province, China in 2011 [18], and the SSO/SSR among power electronic converter-interfaced wind generators in Hami, Xinjiang, China in 2015 [19], [20]. These incidents have revealed a pressing need to investigate the emerging SSO/SSR phenomena. At present, there are some task forces in IEEE which focus on the SSO/SSR phenomena, such as the "IEEE wind SSO Task Force" established in 2017 [21] and the "IEEE PES Task Force on Oscillation Source Location" [22]. Some academic activities on SSO/SSR issues have also been organized recently, such as the Wind SSO Task Force Committee Meeting at 2018 IEEE PES General Meeting [23]. According to the IEEE report, SSR refers to the oscillation resulting from the interactions of the turbine-generator with series compensation equipment, while SSO refers to the oscillation resulting from the interactions of the turbine-generator with quick acting control devices [24]. However, with the appearance of many new types of SSO/SSR, the conventional classification may be no longer applicable. The authors in [25] make the attempts to refine the classification of SSO/SSR based on the oscillation modes. Specifically, the SSO/SSR is divided into three types according to [25]: (i) SSO/SSR caused by the torsional vibration of rotating machines; (ii) SSO/SSR caused by the electric resonance between the capacitance and the inductance in the power grid, especially the reactive power compensation and filtering devices; (iii) SSO/SSR caused by the interactions of the various converters with the AC grid or other converters. Reference [26] reveals some characteristics of the SSO/SSR caused by the type-3 and type-4 wind farms through analyzing the real-life measurement data.

As another form of the oscillation, LFO is an inherent phenomenon in power systems, which initially originates from the small-signal stability issues of synchronous generators in power grids. Over the past years, more LFO events have occurred in power grids all over the world: for example, the LFO phenomena have been observed at different frequencies in Texas [27]; [28] reports that one LFO incident happened in the south power grid of China in 2005; [29] presents the LFO observation at 0.38 Hz in 2013 summer in the US. These incidents have also aroused the interest of some researchers; in recent years, there have been some studies on LFO, such as the LFO energy flow analyzed in [30] and [31], and the analysis of the damping contribution in [32]. Typically, the LFO can be classified into two types: the local-mode LFO and the inter-area LFO [33], and the latter is of more general concerns. LFO can be suppressed by using power system stabilizers (PSSs) [34], which sets a high requirement for the accuracy of the identification of LFO characteristics. However, with the increasing number of power electronics being connected to the power grid, the LFO modes show more complexities, such as the LFO caused by the integration of renewable energy generations in [35], and the LFO existing in the train-traction network in [36] and [37]. Similar to the SSO/SSR, these emerging LFO phenomena can be seen as the interactions of the power electronics with AC power grids or even other power electronics. Generally, the LFO and the SSO/SSR have different frequency ranges of interests. The LFO can occur at the very low frequency, even as low as 0.1 Hz [38], while the

frequency range of the SSO/SSR is normally higher than the LFO.

In the existing literature, the stability problem caused by the oscillation in power systems is usually known as "oscillatory stability" [39]–[43]. In this paper, the academic terminology "oscillatory stability" is adopted. The eigenvalue-based analysis is a fundamental and conventional method for the power system stability analysis, which is available for both model-based and measurement-based assessment of the oscillatory stability in the power grid [44], [45]. The damping essentially characterizes the decaying rate of the oscillation, which is related to the real part of the eigenvalue [46]. The state-space modeling is widely adopted in the eigenvalue-based analysis, and the advantage is that it can handle the nonlinear system modeling for the stability analysis. References [47]–[51] adopt the state-space modeling approach to built the state-space matrix and use the eigenvalues of the state-space matrix to assess the oscillatory stability in power systems with wind power integration, PV power integration and new transmission technologies. However, the eigenvalue-based oscillatory stability analysis has some limitations: (i) in order to calculate the eigenvalues of the state-space matrix, the space-state model of the system needs to be derived firstly. The large number of power electronics and the complexity of the network topology lead to the consequence that the dimension of the state-space matrix becomes very high [45], which has significantly raised the modeling difficulty as well as the computational burden of computers and affected the efficiency of stability studies [52], [53]; (ii) in addition, the eigenvalue-based analysis cannot effectively reveal the physical mechanism of the emerging oscillation phenomena in a wide frequency range of interests [14].

Apart from the eigenvalue-based analysis method, the impedance-based analysis is also an important approach to assess the stability of the emerging oscillations caused by power electronics integration into power systems [54]. Compared with the eigenvalue-based analysis, the impedance models of each power device are derived individually in the impedance-based analysis, which can effectively reduce the dimension of the formulated models. The impedance model is essentially the transfer function of the power device, where the current variation and voltage variation are considered as the input variable and output variable respectively. The impedance-based analysis can characterize and reveal the mechanism of the oscillatory stability based on the circuit theory.

C. STRUCTURE OF THIS PAPER

In the following sections, a comprehensive review on the impedance-based oscillatory stability analysis is conducted based on its methodology framework as illustrated in Figure 2. The rest of the paper is organized as follows. In Section II, the derivation of impedance models of the power electronic converter-connected equipment is surveyed. Section III presents the characteristics of impedance models in the common coordinate systems. In Section IV and Section V, the lumped impedance model of the whole system/subsystem and the impedance-based oscillatory stability criterion are introduced, respectively. Conclusions are drawn finally in Section VI.

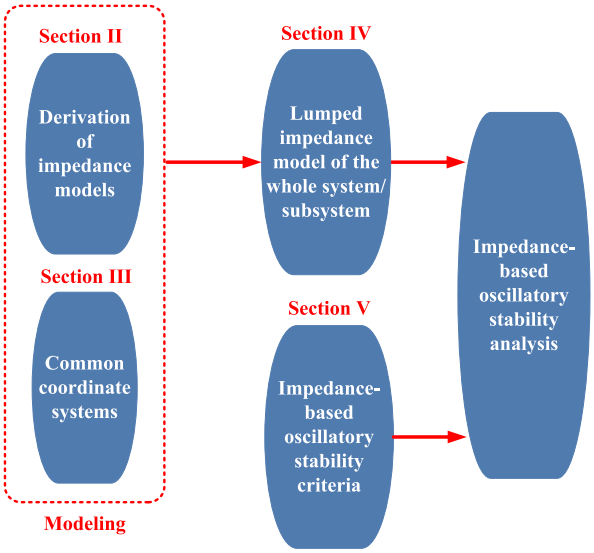

FIGURE 2. Methodology framework of the impedance-based oscillatory stability analysis.

II. DERIVATION OF IMPEDANCE MODELS OF POWER ELECTRONIC CONVERTER-CONNECTED EQUIPMENT

Power systems usually consist of different types of electrical equipment, and some of them are connected with the power electronic converters [55]. Generally, the impedance models of each device (i.e., conventional and power electronic converter-connected equipment) are derived separately, and then the individual impedance models are aggregated into a lumped impedance model of the whole system/subsystem.

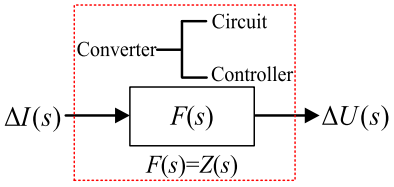

FIGURE 3. External characteristic of the power electronic converter.

A. APRINCIPLE OF IMPEDANCE MODELING OF POWER ELECTRONIC CONVERTERS

The impedance-based oscillatory stability analysis focuses on the external characteristic of the power electronic converter in frequency domain, which is shown in Figure 3. When modeling the power electronic converters (e.g., AC-DC, DC-AC, DC-DC), the following two parts are considered: (i) the circuit dynamics; (ii) the controller dynamics. In other words, both the circuit and the controller have the impact on

the specific equation of the impedance model. In Figure 3, $F(s)$ represents the transfer function; $\Delta I(s)$ represents the current variation in frequency domain; $\Delta U(s)$ represents the voltage variation in frequency domain; $Z(s)$ represents the external characteristic of the power electronic converter, i.e., the impedance model. $F(s)$ usually has the form of the polynomial fraction shown by (1). It should be noted that if $\Delta U(s)$ is considered as the input and $\Delta I(s)$ as the output, $F(s)$ becomes the admittance model $Y(s)$ ($Y(s) = Z(s)^{-1}$). Both models are feasible, but when aggregating the individual impedance/admittance models into a lumped model in the network topology, all individual models should have the same unit, i.e., the unit of models should be unified as "Ω" or "S".

$$F(s) = \frac{\sum_{i=0}^{m} a_i s^i}{\sum_{j=0}^{n} b_j s^j} \tag{1}$$

where a_i and b_j denote the polynomial coefficients; m and n denote the highest power of the polynomial; and s denotes the Laplace operator.

$\Delta I(s)$ and $\Delta U(s)$ in Figure 3 are "virtual settings" in the derivation, and the purpose is to make the transfer function present the characteristics of impedance. What we should do is to derive the relationship between the virtual input/output ($\Delta I(s)$ and $\Delta U(s)$) and the actual variables of the control algorithm, which is shown as the schematic diagram in Figure 4. In fact, the above mentioned "virtual settings" can be changed according to the purpose of the research work; for instance, if both virtual input and output are seen as current deviations, the transfer function presents the characteristics of the dimensionless physical parameter.

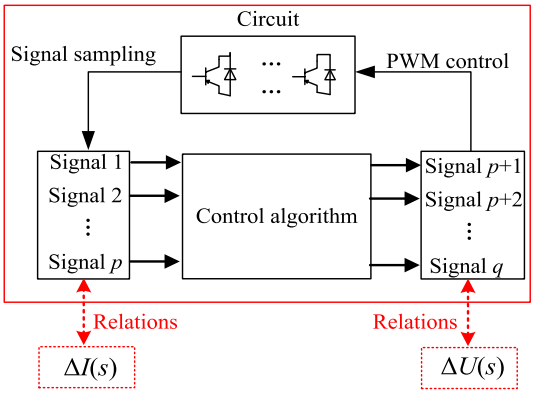

FIGURE 4. Schematic diagram of relationship of input and output.

In the current published research, the impedance models of power electronic converters can be established through the measurement-based method or the derivation-based method. Specifically, the impedance modeling can be classified into the following three conditions according to the availability of the internal structures and control parameters of power electronic converters:

Condition 1 (black-box modeling): for the power electronic converters of which internal structures and control parameters are not available due to the confidential factors, the "black-box" modeling can be employed. The voltage and current variations are measured at the terminals of the power electronic converters in a wide frequency range after imposing the perturbation (i.e., the sweep frequency test), and then the resistance-frequency curve and reactance-frequency curve can be plotted using the measured data. Finally, the impedance model can be determined by the curve-fitting techniques. Reference [56] gives the technical details of the sweep frequency test techniques.

Condition 2 (grey-box modeling): for the power devices of which the limited information about the internal structures and control algorithm is available, the "grey-box" modeling can be employed. In this condition, the "black-box" modeling can also be a choice actually, but it cannot properly identify the control parameters of power electronic devices. Reference [57] estimates the controller parameters of the inverter based on the limited information on the control algorithm as well as the measured data using the system identification techniques, and then derives the equation of the impedance model based on the control parameters. Reference [58] demonstrates the phasor measurement unit (PMU)-based method to identify the parameters of the proposed "Γ equivalent circuit" for the voltage source converter (VSC)-HVDC link, which can be regarded as an application of the "grey-box" modeling.

Condition 3 (white-box modeling): for the power devices of which complete internal structures and control parameters can be obtained, the "white-box" modeling can be employed. The impedance model of power electronic converters needs to be built according to specific circuit structures and corresponding control algorithms. Numerous research reveals that the equation of the impedance model would become more complicated if more complex control loops are involved in the controller (e.g., the research in [59] and [60]). Reference [61] provides an iterative approach to determine the impedance model at given frequency points, which can eliminate some complicated derivations, but it increases the computational burden.

A very effective method from the existing literature to implement the "white-box" modeling for power electronic converters is reviewed in the Subsection II.B.

B. AN EFFECTIVE DERIVATION METHOD

The state-space modeling approach is widely adopted in the stability analysis of power systems. As reported in [62]–[66], the state-space modeling is an effective way to characterize the relationship between the terminal current variation and terminal voltage variation, i.e., the impedance model. The small-signal state-space representation of the power electronic converter is shown in (2).

$$\begin{cases} \Delta \dot{\boldsymbol{x}} = \boldsymbol{A}\Delta \boldsymbol{x} + \boldsymbol{B}\Delta \boldsymbol{u} \\ \Delta \boldsymbol{y} = \boldsymbol{C}\Delta \boldsymbol{x} + \boldsymbol{D}\Delta \boldsymbol{u} \end{cases} \tag{2}$$

where $\Delta \boldsymbol{x}$, $\Delta \boldsymbol{y}$ and $\Delta \boldsymbol{u}$ denote the variations of the state variables, the output variables and the input variables, respectively; $\boldsymbol{A}$, $\boldsymbol{B}$, $\boldsymbol{C}$ and $\boldsymbol{D}$ denote the coefficient matrices with corresponding dimensions.

Typically, the terminal current variation in dq frame ($\Delta \boldsymbol{i}_{\boldsymbol{dq}}$) is set as $\Delta \boldsymbol{u}$ and the terminal voltage variation in dq frame ($\Delta \boldsymbol{u}_{\boldsymbol{dq}}$) is set as $\Delta \boldsymbol{y}$, and then (2) can be replaced by (3).

$$\begin{cases} \Delta \dot{\boldsymbol{x}} = \boldsymbol{A} \Delta \boldsymbol{x} + \boldsymbol{B} \Delta \boldsymbol{i}_{\boldsymbol{dq}} \\ \Delta \boldsymbol{u}_{\boldsymbol{dq}} = \boldsymbol{C} \Delta \boldsymbol{x} + \boldsymbol{D} \Delta \boldsymbol{i}_{\boldsymbol{dq}} \end{cases} \tag{3}$$

By using the Laplace transformation and eliminating the $\Delta \boldsymbol{x}$, the relations in (4) can be derived. The impedance model can be described by (5).

$$\Delta \boldsymbol{u}_{\boldsymbol{dq}}(s) = [\boldsymbol{C}(s) \times (s\boldsymbol{I} - \boldsymbol{A}(s))^{-1} \boldsymbol{B}(s) + \boldsymbol{D}(s)] \Delta \boldsymbol{i}_{\boldsymbol{dq}}(s) \tag{4}$$

$$\boldsymbol{Z}(s) = \boldsymbol{C}(s) \times (s\boldsymbol{I} - \boldsymbol{A}(s))^{-1} \boldsymbol{B}(s) + \boldsymbol{D}(s) \tag{5}$$

where $\boldsymbol{Z}(s)$ denotes the impedance model; $\boldsymbol{I}$ denotes the identity matrix; and s denotes the Laplace operator.

It can be revealed that the state-space modeling is a very straight-forward technique to derive the impedance model. The steps can be summarized as follows: (i) transferring (3) from time domain to frequency domain using Laplace transformation; (ii) deriving $\boldsymbol{A}(s)$, $\boldsymbol{B}(s)$, $\boldsymbol{C}(s)$ and $\boldsymbol{D}(s)$by establishing the frequency-domain model of the individual power electronic converter and considering the voltage variation and current variation as the output variable and input variable respectively; (iii) applying (5) to determine the impedance model.

C. EXAMPLES OF MODELING SOME TYPICAL POWER ELECTRONIC CONVERTER-CONNECTED EQUIPMENT

In this subsection, the impedance models of some typical power electronic converter-connected equipment are reviewed, including the type-3 wind farm equipment, the type-4 wind farm equipment and the HVDC transmission equipment.

1) TYPE-3 WIND FARM EQUIPMENT

The type-3 wind farm is a favorable and mature technique in the wind power industry [67]. The type-3 wind turbine generator is commonly known as the doubly-fed induction generator (DFIG) [26], which is essentially an asynchronous machine. The rotor and stator winding of DFIG are excited by AC sources at different frequencies [68]. The main elements of the type-3 wind farm equipment include the DFIG, the rotor-side converter (RSC) and the grid-side converter (GSC). The structure diagram of the type-3 wind farm is shown in Figure 5.

As the DFIG is coupled into the AC network, the DFIG, RSC and GSC should be considered for the impedance model of type-3 wind farm equipment [69]. The equivalent circuit of DFIG is displayed in Figure 6 [69], where x_m is the mutual reactance of DFIG; r_r is the rotor resistance; x_r is the rotor reactance; r_s is the stator resistance; x_s is the stator reactance; v_{rsc} is the RSC-side equivalent voltage; and S is the slip ratio.

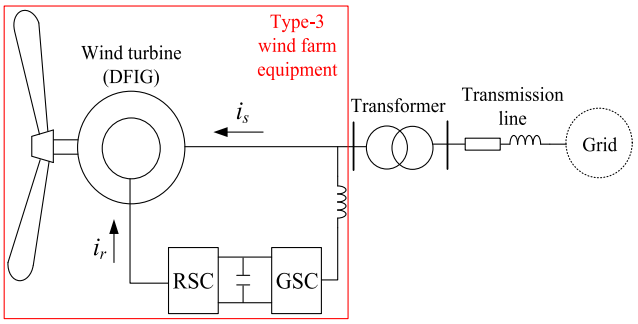

FIGURE 5. Structure diagram of type-3 wind farm [17].

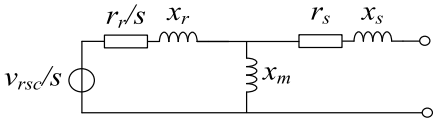

FIGURE 6. Equivalent circuit of DFIG [69].

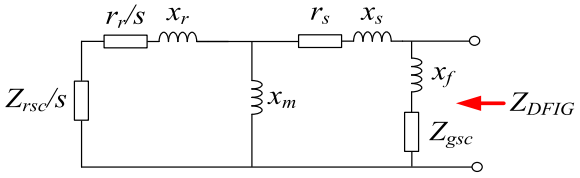

FIGURE 7. Equivalent circuit of whole type-3 wind farm equipment considering RSC and GSC [70], [71].

The slip ratio should be transferred to the frequency domain for the stability analysis. References [70] and [71] propose the equivalent circuit model of the whole type-3 wind farm equipment considering RSC and GSC as shown in Figure 7. In this figure, Z_{rsc} is the impedance model of RSC; Z_{gsc} is the impedance model of GSC; x_f is the filter; and Z_{DFIG} is the impedance model of the whole type-3 wind farm equipment. Z_{rsc} and Z_{gsc} can be derived using the method introduced in Subsection II.B. The impedance model of the whole type-3 wind farm equipment can be obtained based on the series-parallel connection in Figure 7.

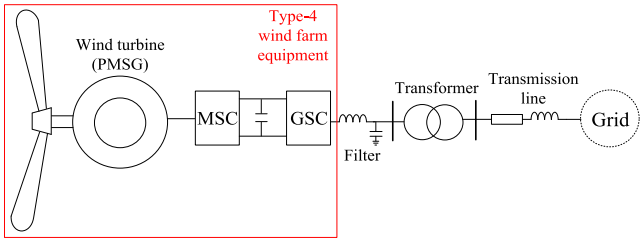

FIGURE 8. Structure diagram of type-4 wind farm [64].

2) TYPE-4 WIND FARM EQUIPMENT

The type-4 wind turbine generator is commonly known as the permanent magnet synchronous generator (PMSG) [26], which is an emerging and promising technique in the wind power industry. The structure diagram of the type-4 wind farm is given by Figure 8; the main elements of the

type-4 wind farm equipment include the PMSG, the machine-side converter (MSC) and the grid-side converter (GSC). However, unlike the type-3 wind farm equipment, the PMSG is decoupled from the AC network by the DC capacitor [72]. That is to say, the PMSG and MSG have no direct interaction with the AC grid as the interaction is blocked by the DC capacitor [73]. Therefore, the main potential oscillation source of the type-4 wind farm is the GSC, and thus the impedance model of GCS is used to represent the impedance model of the whole type-4 wind farm equipment [64]. The impedance model of GSC can be derived by using the method in Subsection II.B.

There are some similarities in oscillation characteristics between the large-scale PV plant and the PMSG-based wind farm, since the similar converter structure and control algorithm are adopted in both large-scale PV plant and PMSG-based wind farm [42]. Therefore, they inevitably have similar impedance model representations, and the modeling of the former would not be repeated here as a result.

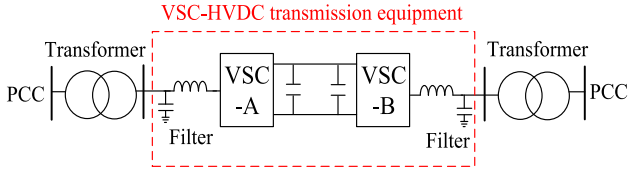

FIGURE 9. Structure diagram of VSC-HVDC transmission equipment [75].

3) HVDC TRANSMISSION EQUIPMENT

VSC-HVDC transmission has become a more attractive technology to integrate the large amount of renewable energy generations to the utility grid [74]. Figure 9 presents a structure diagram of the VSC-HVDC transmission equipment [75], where VSC-A is usually known as the ''rectifier station'' and VSC-B as the ''inverter station''; and PCC denotes the point of common coupling. Reference [76] verifies that the DC-link capacitor has a significant impact on the oscillatory stability. The oscillations caused by the VSC-HVDC transmission technically contains several scenarios: the interaction of rectifier with the external grid that is connected to the rectifier-side PCC; the interaction of inverter with the utility grid that is connected to the inverter-side PCC; the interaction between the two VSCs. The specific case studies are comprehensively provided in [77]–[79]. Therefore, the impedance modeling of the VSC-HVDC transmission equipment depends on the specific oscillation problem under investigation.

D. SOME DISCUSSIONS ON MODULAR POWER ELECTRONIC DEVICES

The modular multi-level converter (MMC) is an emerging technology, which is preferred for the high-voltage, high-power and long-distance transmission in power grids. As reported in [80] and [81], the MMC contains many sub-modules (SMs) with complex internal dynamics and thus the direct derivation of the impedance model could be quite perplexed and ineffective. On this basis, the simplified equivalent circuit model becomes an alternative solution. References [80]–[82] propose the simplified equivalent circuit model of the MMC. Reference [83] analyzes the operation processes of the normal condition and DC fault blocking condition with more details. Reference [84] reveals that the time delay is relatively long in the MMC compared with small-scale power electronics.

The derivation of the impedance model for modular power electronic converters might be quite cumbersome if the ''white-box'' modeling is used and need rely on some equivalence and simplification of its original topology structure to a large extent owing to the large number of SMs, which may however lead to the reduction of the accuracy unavoidably.

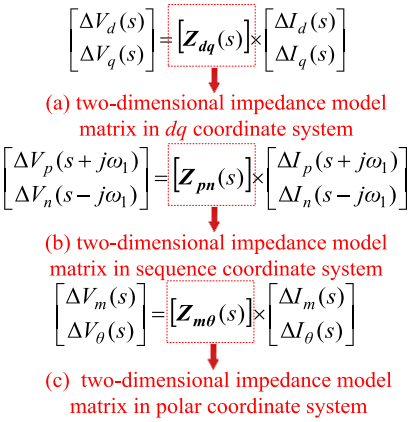

FIGURE 10. Impedance model in three common coordinate systems.

III. IMPEDANCE MODEL DERIVATION IN DIFFERENT COORDINATE SYSTEMS

The impedance model can be derived in different coordinate systems. The common coordinate systems for the impedance model derivation of three-phase power electronic converter-connected equipment include the dq coordinate system, the sequence coordinate system, and the polar coordinate system (e.g., the research in [85]–[89]). As illustrated in Figure 10, the common aim of the impedance model derivation in the three coordinate systems is to characterize the relationship between the terminal current variation and terminal voltage variation but the specific equations of voltage vectors and current vectors are totally different and thus the derivation results of the impedance model are inevitably different in different coordinate systems. In Figure 10, ΔI_d, ΔI_q, ΔV_d and ΔV_q denote the terminal current variation and terminal voltage variation in d axis and q axis, respectively; ΔI_p, ΔI_n, ΔV_p and ΔV_n denote the terminal current variation and terminal voltage variation in positive sequence and negative sequence, respectively; ΔI_m, ΔI_θ, ΔV_m and ΔV_θ denote the terminal current variation and terminal voltage variation in terms of magnitudes and angles, respectively; ω_1 denotes the fundamental angular frequency; $\boldsymbol{Z_{dq}}(s)$ denotes the impedance model in dq coordinate system; $\boldsymbol{Z_{pn}}(s)$ denotes the impedance

model in sequence coordinate system; and $\boldsymbol{Z_{m\theta}}(s)$ denotes the impedance model in polar coordinate system. The current variation and voltage variation are always two-dimensional vectors and hence in any of the aforementioned coordinate systems, the impedance models are two-dimensional matrices to describe the external characteristic of three-phase power electronic converters [90], [91].

TABLE 1. Characteristics of impedance models in different coordinate systems.

	Impedance Model of VSC	Impedance Model of *R-L* Transmission Line
DQ Coordinate System	$\begin{bmatrix}\odot & \odot\\ \odot & \odot\end{bmatrix}_{2\times2}$	$\begin{bmatrix}\odot & \odot\\ \odot & \odot\end{bmatrix}_{2\times2}$
Sequence Coordinate System	$\begin{bmatrix}\odot & \odot\\ \odot & \odot\end{bmatrix}_{2\times2}$	$\begin{bmatrix}\odot & \otimes\\ \otimes & \odot\end{bmatrix}_{2\times2}$
Polar Coordinate System	$\begin{bmatrix}\odot & \otimes\\ \otimes & \odot\end{bmatrix}_{2\times2}$	$\begin{bmatrix}\odot & \odot\\ \odot & \odot\end{bmatrix}_{2\times2}$

Note: ⊙denotes non-zero elements; ⊗represents zero elements.

It is important to have an intuitive understanding for the impedance models in different coordinate systems. In [88] and [91], the characteristics of impedance models of the VSC and *R-L* transmission line in *dq* coordinate system, sequence coordinate system and polar coordinate system are analyzed, which is summarized in Table 1. The following findings can be summarized: (i) the impedance models of VSC and *R-L* transmission line in *dq* coordinate system are both two-dimensional and non-diagonal matrices; (ii) the impedance model of VSC in sequence coordinate system is a two-dimensional and non-diagonal matrix, but the impedance model of *R-L* transmission line in the sequence coordinate system is a two-dimensional and diagonal matrix; (iii) the impedance model of VSC in polar coordinate system is a two-dimensional and diagonal matrix under the assumption that the power factor of the VSC is 1, but the impedance model of *R-L* transmission line in the polar coordinate system is a two-dimensional and non-diagonal matrix.

Taking the three-phase *R-L* transmission line as an example, its impedance models in different coordinate systems are shown as follows.

(i) In *dq* coordinate system:

$$Z_{line}^{(1)} = \begin{bmatrix} R + sL & -\omega L \\ \omega L & R + sL \end{bmatrix} \tag{6}$$

(ii) In sequence coordinate system:

$$Z_{line}^{(2)} = \begin{bmatrix} R + sL + \mathrm{j}\omega L & 0 \\ 0 & R + sL - \mathrm{j}\omega L \end{bmatrix} \tag{7}$$

(iii) In polar coordinate system (8), as shown at the bottom of this page, where $Z_{line}^{(1)}$, $Z_{line}^{(2)}$ and $Z_{line}^{(3)}$ are the impedance models of the three-phase *R-L* transmission line in *dq* coordinate system, sequence coordinate system and polar coordinate system, respectively; V denotes the terminal voltage of the *R-L* transmission line; and I denotes the current of the *R-L* transmission line.

In fact, the equations of the impedance model in *dq* coordinate system and sequence coordinate system are interchangeable. In [87] and [88], the mutual transformation of the impedance model between *dq* coordinate system and sequence coordinate system is revealed, which can be shown by (9)-(12).

$$\boldsymbol{Z_{dq}} = \boldsymbol{T}^{-1}\boldsymbol{Z_{pn}}\boldsymbol{T} \tag{9}$$

$$\boldsymbol{Z_{pn}} = \boldsymbol{T}\boldsymbol{Z_{dq}}\boldsymbol{T}^{-1} \tag{10}$$

$$\boldsymbol{T} = \frac{1}{\sqrt{2}}\begin{bmatrix} 1 & \mathrm{j} \\ 1 & -\mathrm{j} \end{bmatrix} \tag{11}$$

$$\boldsymbol{T}^{-1} = \frac{1}{\sqrt{2}}\begin{bmatrix} 1 & 1 \\ -\mathrm{j} & \mathrm{j} \end{bmatrix} \tag{12}$$

where $\boldsymbol{Z_{dq}}$ denotes the impedance model in *dq* coordinate system; $\boldsymbol{Z_{pn}}$ denotes the impedance model in sequence coordinate system; and $\boldsymbol{T}$ denotes the transformation matrix.

Since each power electronic converter is controlled in its individual *dq* frame determined by the phase locked loop, with the co-existence of multiple grid-connected power electronic converters, the unified/global *dq* frame for the whole power system analysis is required and proposed in [63] and [92] so that each impedance model is adjusted from its individual *dq* frame to the unified/global *dq* frame.

IV. LUMPED IMPEDANCE MODEL OF WHOLE SYSTEM/SUBSYSTEM

The impedance model of each electrical element is the separate matrix, which needs to be aggregated into a lumped impedance model for the oscillatory stability assessment of the whole system/subsystem using the stability criterion introduced in Section V.

Regarding the treatment of the impedance network, a typical procedure is described as follows: firstly, the isolated impedance models of corresponding electrical elements are connected together to form the impedance network of the actual topology as shown in Figure 11(b), which should be consistent with the actual location of electrical elements in the grid network (Figure 11(a)). Then, the impedance network is

$$Z_{line}^{(3)} = \begin{bmatrix} |R + \mathrm{j}\omega L| + sL\cos[-\arg(R + \mathrm{j}\omega L)] & -sLI\cos[-\arg(R + \mathrm{j}\omega L)] \\ \dfrac{sL\sin[-\arg(R + \mathrm{j}\omega L)]}{V} & 1 + \dfrac{sL\cos[-\arg(R + \mathrm{j}\omega L)]}{|R + \mathrm{j}\omega L|} \end{bmatrix} \tag{8}$$

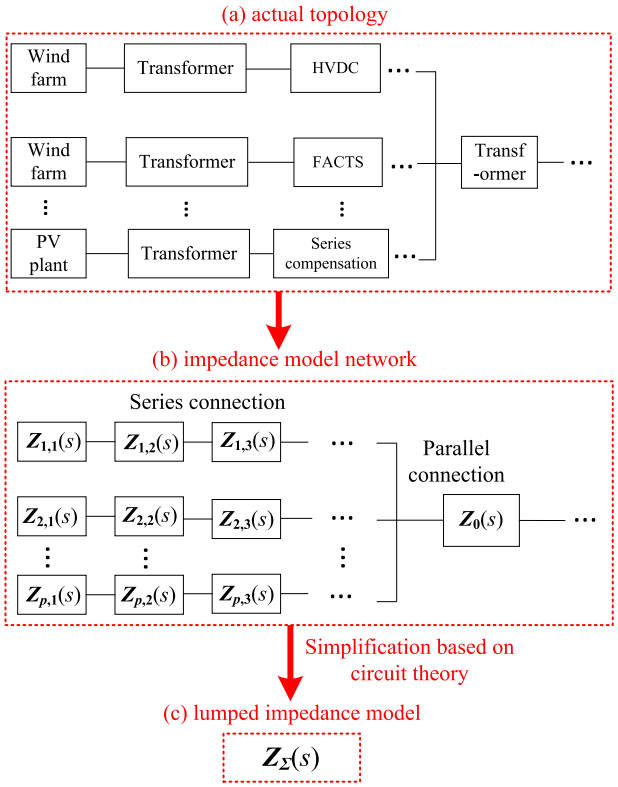

FIGURE 11. Schematic diagram of treatment of impedance network.

simplified according to the series-parallel connection relation of each electrical element to derive the lumped impedance model of the whole system/subsystem in Figure 11 (c). The lumped impedance model is expressed by (13), which is a two-dimensional matrix.

$$\boldsymbol{Z}_{\boldsymbol{\Sigma}}(s) = \begin{bmatrix} z_{\Sigma-11}(s) & z_{\Sigma-12}(s) \\ z_{\Sigma-21}(s) & z_{\Sigma-22}(s) \end{bmatrix} \tag{13}$$

where $\boldsymbol{Z}_{\boldsymbol{\Sigma}}(s)$ denotes the lumped impedance model in frequency domain; $Z_{\Sigma-11}(s)$, $Z_{\Sigma-12}(s)$, $Z_{\Sigma-21}(s)$ and $Z_{\Sigma-22}(s)$ denote the four elements of the lumped impedance model matrix. Please note that the concept of the subsystem mainly appears in Nyquist criterion. Nyquist criterion focuses more on the oscillation of the local area and splits the local area into source subsystem and non-source subsystem. Taking an example, the wind farm, transformer and rectifier-side HVDC equipment in Figure 11(a) can be regarded as a local area with the wind farm as the source subsystem and transformer & HVDC as the non-source subsystem. The scale of subsystems is usually small and the subsystems are generally assumed to be stable themselves. *R-X* criterion focuses more on the oscillation of the global area, and there may be multiple oscillation modes in a comparatively larger area. *R-X* criterion can operate in the quantitative manner. Details of Nyquist criterion and *R-X* criterion will be discussed in Section V.

The authors in [93] provides another way to deal with the impedance network, and the key step is to formulate the lumped state-space model. Specifically, in [93], the state-space models of each power device are derived separately. Then, an algebra interconnection method is proposed to combine different power devices, where only input-output relationship is concerned and the lumped state-space model of the whole system/subsystem is reformulated in a computationally-efficient way. Finally, the impedance model of the whole system/subsystem can be obtained from the matrices of the lumped state-space model.

V. IMPEDANCE-BASED OSCILLATORY STABILITY CRITERIA

There are two commonly-used impedance-based oscillatory stability criteria: (i) Nyquist criterion; (ii) *R-X* criterion. The technical details of these two criteria are summarized as follows.

A. NYQUIST-CRITERION-BASED OSCILLATORY STABILITY ASSESSMENT

As discussed in Section IV, for the Nyquist-criterion-based oscillatory stability assessment, the local system should be split into two subsystems firstly: the source subsystem and the non-source subsystem [94], which are displayed in Figure 12. When the two subsystems oscillate with each other with negative damping, the oscillation in the interconnected subsystems will be diverged, i.e., the unstable oscillation happens.

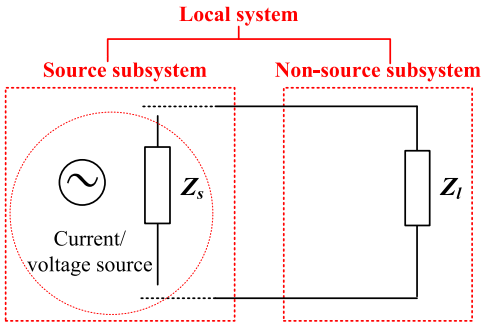

FIGURE 12. Two subsystems for Nyquist-criterion-based oscillatory stability assessment.

As reported in [95] and [96], assuming that the power devices themselves are stable, the system stability depends on the positions of the set of $\boldsymbol{\lambda}(s)$ (see (14)) on the complex plane. The impedance ratio matrix is defined by (15). Due to the fact that $\boldsymbol{Z}_s(s)$ and $\boldsymbol{Z}_l(s)$ are the 2×2 matrices, the form of $\boldsymbol{R}(s)$ is also the 2×2 matrix.

$$\det[\boldsymbol{\lambda}(s)\boldsymbol{I} - \boldsymbol{R}(s)] = 0 \tag{14}$$

$$\boldsymbol{R}(s) = \begin{cases} \boldsymbol{Z}_{\boldsymbol{l}}(s)\boldsymbol{Y}_{\boldsymbol{s}}(s) & \text{(Case in Fig.13(a))} \\ \boldsymbol{Z}_{\boldsymbol{s}}(s)\boldsymbol{Y}_{\boldsymbol{l}}(s) & \text{(Case in Fig.13(b))} \end{cases} \tag{15}$$

where $\boldsymbol{R}(s)$ denotes the impedance ratio matrix; $\boldsymbol{Z}_l(s)$ (or $\boldsymbol{Y}_l(s)$) denotes the non-source-side impedance model (or admittance model); $\boldsymbol{Z}_s(s)$ (or $\boldsymbol{Y}_s(s)$) denotes the source-side impedance model (or admittance model); $\boldsymbol{I}$ denotes the identity matrix; $\boldsymbol{\lambda}(s)$ denotes the set of eigenvalues in a wide frequency range. It is noted that $\boldsymbol{Y}(s) = \boldsymbol{Z}(s)^{-1}$.

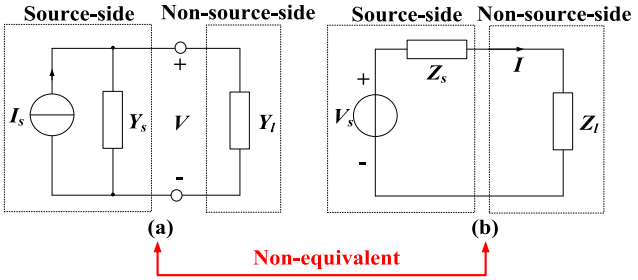

FIGURE 13. Two types of small-signal representation for Nyquist-criterion-based oscillatory stability assessment [97].

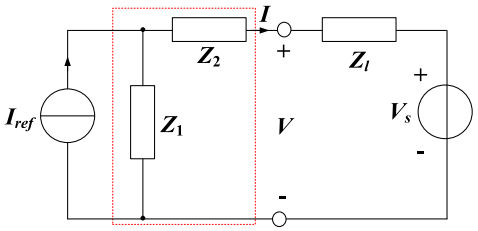

FIGURE 14. Reconstructed small-signal representation circuit [99].

The mechanism of the Nyquist criterion is to identify the location of eigenvalues, which is widely adopted to assess the oscillatory stability issues in the power system. It is assumed that the current/voltage source in Figure 13 is stable when unloaded, and the $\boldsymbol{Z}_l$ (or $\boldsymbol{Y}_l$) in Figure 13 is stable when supplied by an ideal voltage/current source. If the Nyquist curve of the impedance ratio satisfies the Nyquist criterion (i.e., the Nyquist curves do not clockwise surround the point $(-1, 0)$), the system is stable. The impedance ratio can be $\boldsymbol{Z}_s/\boldsymbol{Z}_l$ or $\boldsymbol{Z}_l/\boldsymbol{Z}_s$, which depends on the feature of the source-side subsystem.

As illustrated in [97], the grid-connected inverter is usually controlled as the current source. Therefore, most literature considers the small-signal representation of the grid-connected inverter as an ideal current source with an internal parallel-connected admittance (or impedance), as shown in Figure 13(a). If the source-side subsystem show the features of the voltage source, its small-signal representation can be regarded as an ideal voltage source with the series-connected impedance, which is shown in Figure 13(b); [98] indicates that the converter under the virtual synchronous generator (VSG) mode usually behaves like a voltage source. As also indicated in [97], the small-signal representation of a specific subsystem in Figure 13(a) cannot be transferred to that in Figure 13(b) and vice versa; the reasons are discussed in [97].

As discussed in [99], when the converter adopts the adaptive control with time-varying parameters, the ideal current source I_s may become unstable, which breaks the assumption and may bring errors to the assessment result. Therefore, a reconstructed small-signal representation is proposed in [99], which is shown in Figure 14. The Nyquist curve of $(\boldsymbol{Z}_2+\boldsymbol{Z}_l)/\boldsymbol{Z}_1$ should satisfy the Nyquist criterion to guarantee the system stability. I_{ref} is the reference value for the current, and (16) should be satisfied to ensure the consistency with Figure 13(a).

$$\boldsymbol{Z}_s = \boldsymbol{Z}_1 + \boldsymbol{Z}_2 \tag{16}$$

Nyquist criterion is effective for the oscillatory stability assessment of the local area. However, it is not easy to identify and determine the source subsystem and non-source subsystem for the large-scale multi-machine systems, and it should be guaranteed that there is no instability in the subsystems. Moreover, the Nyquist criterion cannot provide the deep explanation of the oscillation phenomena from the perspective of the oscillatory mechanism. Finally, the Nyquist criterion cannot effectively operate in the quantitative manner.

B. R-X-CRITERION-BASED OSCILLATORY STABILITY ASSESSMENT

The *R-X* criterion is an alternative method to assess the oscillatory stability, where *R* refers to the resistance part of the impedance model and *X* refers to the reactance part of the impedance model. The *R-X* criterion can quantificationally assess the oscillatory stability based on the circuit theory.

The real part of the impedance model (i.e., the $R(s)$) and the imaginary part of the impedance model (i.e., the $X(s)$) form the foundation of the *R-X* criterion. The *R-X* criterion is briefly derived and discussed in [63], [65], [100]. The oscillatory stability can be quantificationally evaluated by plotting and analyzing the reactance-frequency curve and resistance-frequency curve in a wide frequency range. Under the circumstance that $X(s)$ has zero-crossing points within the positive frequency range, (i) if the frequency spectrum curve of $X(s)$ crosses its zero point from negative to positive side (i.e., the slope of $X(s)$ at its zero point is positive) and the value of $R(s)$ at the zero point of $X(s)$ is negative, the undamped oscillation will occur; (ii) if the frequency spectrum curve of $X(s)$ crosses its zero point from positive to negative side (i.e., the slope of $X(s)$ at its zero point is negative) and the value of $R(s)$ at the zero point of $X(s)$ is positive, the undamped oscillation will occur. Reference [56] also indicates that $X(s)$ crosses its zero points from negative to positive side in the series resonance mode, while $X(s)$ crosses its zero points from positive to negative side in the parallel resonance mode.

As discussed in the Section IV, the lumped impedance model is a two-dimensional matrix, which cannot be directly used to plot the resistance-frequency curve and reactance-frequency curve. Therefore, the dimension-reduction for the lumped impedance model matrix are discussed in the following.

The first technique of dimension-reduction is to employ the determinant of the lumped impedance model matrix to represent the one-dimensional impedance [63], [64], which

is given in (17).

$$Z_D(s) = \det[\mathbf{Z_\Sigma}(s)] = Z_{\Sigma-11}(s)Z_{\Sigma-22}(s) - Z_{\Sigma-12}(s)Z_{\Sigma-21}(s) \quad (17)$$

where $Z_D(s)$ denotes the dimension-reduced lumped impedance model in frequency domain; the definitions of $\mathbf{Z_\Sigma}(s)$, $Z_{\Sigma-11}(s)$, $Z_{\Sigma-12}(s)$, $Z_{\Sigma-21}(s)$ and $Z_{\Sigma-22}(s)$ are provided in (13).

The second technique of dimension-reduction is to consider the average value of the d-axis impedance and q-axis impedance in dq frame as the dimension-reduced lumped impedance model [61], [62], [65], and the specific equations are presented in (18)-(20). However, this technique is lack of a deep theoretical support.

$$\begin{bmatrix} \Delta u_d \\ \Delta u_q \end{bmatrix} = \begin{bmatrix} z_{\Sigma-11}(s) & z_{\Sigma-12}(s) \\ z_{\Sigma-21}(s) & z_{\Sigma-22}(s) \end{bmatrix} \cdot \begin{bmatrix} \Delta i_d \\ \Delta i_q \end{bmatrix} \quad (18)$$

$$\begin{aligned} \Delta u_d(s) + \mathrm{j}\Delta u_q(s) &= z_{\Sigma-11}(s) \cdot \Delta i_d(s) + z_{\Sigma-12}(s) \cdot \Delta i_q(s) \\ &\quad + \mathrm{j}\,[z_{\Sigma-21}(s) \cdot \Delta i_d(s) + z_{\Sigma-22}(s) \cdot \Delta i_q(s)] \\ &= [z_{\Sigma-11}(s) + \mathrm{j}\, z_{\Sigma-21}(s)] \cdot \Delta i_d(s) \\ &\quad + \mathrm{j}\,[z_{\Sigma-22}(s) - \mathrm{j}\, z_{\Sigma-12}(s)] \cdot \Delta i_q(s) \quad (19) \end{aligned}$$

$$\begin{aligned} Z_D(s) &= \frac{z_{\Sigma-11}(s) + \mathrm{j}\, z_{\Sigma-21}(s) + z_{\Sigma-22}(s) - \mathrm{j}\, z_{\Sigma-12}(s)}{2} \\ &= \frac{[z_{\Sigma-11}(s) + z_{\Sigma-22}(s)] + \mathrm{j}\,[z_{\Sigma-21}(s) - z_{\Sigma-12}(s)]}{2} \quad (20) \end{aligned}$$

where Δi_d and Δi_q are the terminal current variations in d-axis and q-axis, respectively; and Δu_d and Δu_q are the terminal voltage variations in d-axis and q-axis, respectively.

References [101] and [102] apply the circuit theory with consideration of the coupling to reduce the dimension of the impedance model matrix in the sequence coordinate system and derive the one-dimensional positive sequence impedance and negative sequence impedance respectively, which is the third dimension-reduction technique. It can be noted that the third dimension-reduction technique actually decouples one impedance model matrix to two one-dimensional impedance equations in positive and negative sequences.

The impedance model matrix usually has non-zero non-diagonal elements, and the formula of the dimension-reduced lumped impedance model may have high orders. The $R(s)$ and $X(s)$ are computed based on the dimension-reduced lumped impedance given by (21) and (22). The equations of $R(s)$ and $X(s)$ can be obtained directly through analytical derivation, or the curves of $R(s)$ and $X(s)$ can be obtained by the enumeration for the large number of frequency points, and then the specific equations of $R(s)$ and $X(s)$ can be obtained by the fitting technique. The program can be preset into the computer, and the enumeration operation can be carried out by cyclic procedures.

$$R(s) = \mathrm{Re}[Z_D(s)] \quad (21)$$

$$X(s) = \mathrm{Im}[Z_D(s)] \quad (22)$$

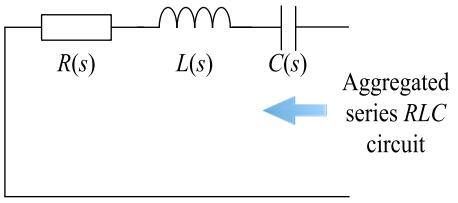

FIGURE 15. Aggregate series *RLC* circuit for series resonance mode [62].

In order to characterize the damping of the series resonance based on the second-order circuit theory, the aggregated series *RLC* circuit is derived in [62] and [103], which is shown in Figure 15. Then, the damping $\sigma(s)$ and the oscillation frequency $\omega(s)$ are computed from (23)-(24) by employing the second-order circuit theory. However, this aggregated series *RLC* circuit cannot characterize and handle the case that the $X(s)$ crosses its zero point from positive to negative side. As discussed, the positive resistance may be the cause of the undamped oscillation for this case, which is also a potential critical mode in power systems.

$$\sigma(s) = \frac{R(s)}{2L(s)} \quad (23)$$

$$\omega(s) = \sqrt{\frac{1}{L(s)C(s)} - \left(\frac{R(s)}{2L(s)}\right)^2} \quad (24)$$

where $L(s)$ and $C(s)$ are the frequency spectrum functions of the equivalent inductance and equivalent capacitance in the wide frequency range, respectively. As illustrated in [104]–[106], there are many uncertainties in power systems and the risk can be examined by analyzing the probabilistic stability of power systems with various uncertainties. The settling time of the oscillation can be calculated based on the damping value (see (25)) [103], which can lay a foundation to establish the risk matrix for the probabilistic analysis.

$$T_s(s) = \frac{3}{\sigma(s)} \quad (25)$$

where $T_s(s)$ denotes the frequency spectrum function of the settling time in the wide frequency range.

VI. CONCLUSION

The evaluation of the oscillatory stability is of great importance to the secure operation of power systems, and the impedance-based analysis provides an effective solution. This paper carries out a systematic review on the published research of the impedance-based oscillatory stability analysis of power systems with high power electronics penetration. Firstly, some technical matters regarding the derivation of impedance models of the power electronic converter-connected equipment are summarized. Then, common coordinate systems for the derivation of the impedance model are introduced, and the characteristics as well as the mutual transformation of the impedance model in different coordinate systems are surveyed. After that, the aggregation of individual impedance models to form the lumped impedance model

is presented. Finally, two typical impedance-based oscillatory stability criteria, i.e., Nyquist criterion and *R-X* criterion, are introduced in details. The following conclusions can be drawn from the systematic survey of the impedance-based oscillatory stability analysis:

Compared with the conventional eigenvalue-based analysis, the impedance-based analysis has some unique advantages: (i) the impedance-based analysis can quantificationally characterize the oscillation phenomena based on the circuit theory in the wide frequency range; (ii) the impedance models of each electrical element are derived separately, which only have two dimensions for the three-phase power devices; that is to say, the low dimensionality can mitigate the modeling difficulty. However, the impedance-based analysis suffers from the similar deficiency as the eigenvalue-based analysis does: the impedance-based analysis is a kind of model-based method, which means that a validated and accurate model is required; for some power electronics with incomplete internal information or some modular power electronics, the accurate impedance model is usually not easy to be obtained.

On the whole, the impedance-based oscillatory stability analysis provides a prominent contribution to the theory of oscillatory stability assessment. It has a great potential and prospect to be generalized to tackle the oscillatory stability in power systems which possess a large population of power electronics. However, there are still some gaps/challenges for the existing studies: (i) more types of renewable power generations should be taken into account in the assessment; (ii) more efficient techniques are expected for the establishment of the impedance model of modular power electronic converters; (iii) the impedance model considering various uncertainty factors are awaited to be developed.

REFERENCES

[1] S. Su, Y. Hu, T. Yang, S. Wang, Z. Liu, X. Wei, M. Xia, Y. Ota, and K. Yamashita, "Research on an electric vehicle owner-friendly charging strategy using photovoltaic generation at office sites in major Chinese cities," *Energies*, vol. 11, no. 2, p. 421, Feb. 2018.

[2] D. Solatialkaran, F. Zare, T. K. Saha, and R. Sharma, "A novel approach in filter design for grid-connected inverters used in renewable energy systems," *IEEE Trans. Sustain. Energy*, to be published.

[3] S. Su, Y. Hu, L. He, K. Yamashita, and S. Wang, "An assessment procedure of distribution network reliability considering photovoltaic power integration," *IEEE Access*, vol. 7, pp. 60171–60185, May 2019.

[4] D. Kumar, V. Gupta, and R. C. Jha, "Implementation of FACTS devices for improvement of voltage stability using evolutionary algorithm," in *Proc. IEEE 1st Int. Conf. Power Electron., Intell. Control and Energy Syst.*, Delhi, India, Jul. 2016, pp. 1–6.

[5] M. Mehrasa, E. Pouresmaeil, S. Zabihi, and J. P. S. Catalão, "Dynamic model, control and stability analysis of MMC in HVDC transmission systems," *IEEE Trans. Power Del.*, vol. 32, no. 3, pp. 1471–1482, Jun. 2017.

[6] Y. Hu, S. Su, L. He, X. Wu, T. Ma, Z. Liu, and X. Wei, "A real-time multilevel energy management strategy for electric vehicle charging in a smart electric energy distribution system," *Energy Technol.*, vol. 7, no. 5, p. 1800705, May 2019.

[7] Y. Cheng and C. Zhang, "Configuration and operation combined optimization for EV battery swapping station considering PV consumption bundling," *Protection Control Mod. Power Syst.*, vol. 2, no. 1, p. 26, Dec. 2017.

[8] M. Zhao, X. Yuan, J. Hu, and Y. Yan, "Voltage dynamics of current control time-scale in a VSC-connected weak grid," *IEEE Trans. Power Syst.*, vol. 31, no. 4, pp. 2925–2937, Jul. 2016.

[9] M. F. Firuzi, A. Roosta, and M. Gitizadeh, "Stability analysis and decentralized control of inverter-based *ac* microgrid," *Protection Control Mod. Power Syst.*, vol. 4, no. 1, p. 6, Dec. 2019.

[10] J. Khazaei, Z. Miao, and L. Piyasinghe, "Impedance-model-based MIMO analysis of power synchronization control," *Electr. Power Syst. Res.*, vol. 154, pp. 341–351, Jan. 2018.

[11] S. Bu, W. Du, and H. Wang, "Model validation of DFIGs for power system oscillation stability analysis," *IET Renew. Power Gener.*, vol. 11, no. 6, pp. 858–866, May 2017.

[12] G. Magdy, G. Shabib, A. A. Elbaset, and Y. Mitani, "Optimized coordinated control of LFC and SMES to enhance frequency stability of a real multi-source power system considering high renewable energy penetration," *Protection Control Mod. Power Syst.*, vol. 3, no. 1, p. 39, Dec. 2018.

[13] Z. Ma, H. Chen, and Y. Chai, "Analysis of voltage stability uncertainty using stochastic response surface method related to wind farm correlation," *Protection Control Mod. Power Syst.*, vol. 2, no. 1, p. 20, Dec. 2017.

[14] K. Gu, F. Wu, and X.-P. Zhang, "Sub-synchronous interactions in power systems with wind turbines: A review," *IET Renew. Power Gener.*, vol. 13, no. 1, pp. 4–15, Jan. 2019.

[15] H. Ghasemi, G. Gharehpetian, S. A. Nabavi-Niaki, and J. Aghaei, "Overview of subsynchronous resonance analysis and control in wind turbines," *Renew. Sustain. Energy Rev.*, vol. 27, pp. 234–243, Nov. 2013.

[16] H. Liu, X. Xie, Y. Li, H. Liu, and Y. Hu, "A small-signal impedance method for analyzing the SSR of series-compensated DFIG-based wind farms," in *Proc. IEEE Power Energy Soc. Gen. Meeting*, Denver, CO, USA, Jul. 2015, pp. 1–5.

[17] L. Fan, R. Kavasseri, Z. L. Miao, and C. Zhu, "Modeling of DFIG-based wind farms for SSR analysis," *IEEE Trans. Power Del.*, vol. 25, no. 4, pp. 2073–2082, Oct. 2010.

[18] H. Liu, X. Xie, Y. Li, H. Liu, and Y. Hu, "Mitigation of SSR by embedding subsynchronous notch filters into DFIG converter controllers," *IET Gener., Transmiss. Distrib.*, vol. 11, no. 11, pp. 2888–2896, Mar. 2017.

[19] Y. Xu and Y. Cao, "Sub-synchronous oscillation in PMSGs based wind farms caused by amplification effect of GSC controller and PLL to harmonics," *IET Renew. Power Gener.*, vol. 12, no. 7, pp. 844–850, May 2018.

[20] Z. Zheng, Z. An, and C. Shen, "Evaluation method for equivalent models of PMSG-based wind farms considering randomness," *IEEE Trans. Sustain. Energy*, vol. 10, no. 3, pp. 1565–1574, Jul. 2019.

[21] *IEEE Wind SSO Taskforce*. Accessed: Jul. 16, 2019. [Online]. Available: https://sites.google.com/view/windsso/home

[22] *IEEE PES Task Force on Oscillation Source Location*. Accessed: Jul. 16, 2019. [Online]. Available: http://web.eecs.utk.edu/~kaisun/TF/index.html

[23] *2018 GM Meeting Summary for Wind SSO Task Force*. Accessed: Jul. 16, 2019. [Online]. Available: https://drive.google.com/file/d/1poga5oLw6eKzi8RfkpJrYNd3N7i-G9pN/view

[24] IEEE Subsynchronous Resonance Working Group, "Reader's guide to subsynchronous resonance," *IEEE Trans. Power Syst.*, vol. 7, no. 1, pp. 150–157, Feb. 1992.

[25] L. Wang, X. Xie, H. Liu, Y. Zhan, J. He, and C. Wang, "Review of emerging SSR/SSO issues and their classifications," *J. Eng.*, vol. 2017, no. 13, pp. 1666–1670, 2017.

[26] X. Xie, X. Zhang, H. Liu, H. Liu, Y. Li, and C. Zhang, "Characteristic analysis of subsynchronous resonance in practical wind farms connected to series-compensated transmissions," *IEEE Trans. Energy Convers.*, vol. 32, no. 3, pp. 1117–1126, Sep. 2017.

[27] J. Chen, P. Shrestha, S.-H. Huang, N. D. R. Sarma, J. Adams, D. Obadina, and J. Ballance, "Use of synchronized phasor measurements for dynamic stability monitoring and model validation in ERCOT," in *Proc. IEEE Power Energy Soc. Gen. Meeting*, San Diego, CA, USA, Jul. 2012, pp. 1–7.

[28] J. Ma, P. Zhang, H.-J. Fu, B. Bo, and Z.-Y. Dong, "Application of phasor measurement unit on locating disturbance source for low-frequency oscillation," *IEEE Trans. Smart Grid.*, vol. 1, no. 3, pp. 340–346, Dec. 2010.

[29] S. A. N. Sarmadi and V. Venkatasubramanian, "Inter-area resonance in power systems from forced oscillations," *IEEE Trans. Power Syst.*, vol. 31, no. 1, pp. 378–386, Jan. 2016.

[30] L. Chen, Y. Min, and W. Hu, "An energy-based method for location of power system oscillation source," *IEEE Trans. Power Syst.*, vol. 28, no. 2, pp. 828–836, May 2013.

[31] Y. Yu, S. Grijalva, J. J. Thomas, L. Xiong, P. Ju, and Y. Min, "Oscillation energy analysis of inter-area low-frequency oscillations in power systems," *IEEE Trans. Power Syst.*, vol. 31, no. 2, pp. 1195–1203, Mar. 2016.

[32] R. Xie and D. J. Trudnowski, "Tracking the damping contribution of a power system component under ambient conditions," *IEEE Trans. Power Syst.*, vol. 33, no. 1, pp. 1116–1117, Jan. 2018.

[33] X. Zhang, C. Lu, S. Liu, and X. Wang, "A review on wide-area damping control to restrain inter-area low frequency oscillation for large-scale power systems with increasing renewable generation," *Renew. Sustain. Energy Rev.*, vol. 57, pp. 45–58, May 2016.

[34] B. Dasu, M. Sivakumar, and R. Srinivasarao, "Interconnected multimachine power system stabilizer design using whale optimization algorithm," *Protection Control Mod. Power Syst.*, vol. 4, no. 1, p. 2, Dec. 2019.

[35] Z. Sun, G. Cai, D. Yang, and C. Liu, "Application of power system energy structures to track dominated oscillation paths and generator damping contribution during low-frequency oscillations," *Int. J. Elect. Power Energy Syst.*, vol. 104, pp. 52–68, Jan. 2019.

[36] Y. Liao, Z. Liu, H. Zhang, and B. Wen, "Low-frequency stability analysis of single-phase system with *dq*-frame impedance approach—Part II: Stability and frequency analysis," *IEEE Trans. Ind. Appl.*, vol. 54, no. 5, pp. 5012–5024, Sep. 2018.

[37] Z. Liu, G. Zhang, and Y. Liao, "Stability research of high-speed railway EMUs and traction network cascade system considering impedance matching," *IEEE Trans. Ind. Appl.*, vol. 52, no. 5, pp. 4315–4326, Sep. 2016.

[38] A. Salgotra and S. Pan, "Model based PI power system stabilizer design for damping low frequency oscillations in power systems," *ISA Trans.*, vol. 76, pp. 110–121, May 2018.

[39] G. Rogers, *Power System Oscillations*. New York, NY, USA: Springer, 2012.

[40] J. L. Rueda, J. C. Cepeda, I. Erlich, A. W. Korai, and F. M. Gonzalez-Longatt, "Probabilistic approach for risk evaluation of oscillatory stability in power systems," in *PowerFactory Applications for Power System Analysis*. Cham, Switzerland: Springer, 2014, pp. 249–266.

[41] J. Shair, X. Xie, and G. Yan, "Mitigating subsynchronous control interaction in wind power systems: Existing techniques and open challenges," *Renew. Sustain. Energy Rev.*, vol. 108, pp. 330–346, Jul. 2019.

[42] R. Shah, N. Mithulananthan, and R. Bansal, "Oscillatory stability analysis with high penetrations of large-scale photovoltaic generation," *Energy Convers. Manage.*, vol. 65, pp. 420–429, Jan. 2013.

[43] J. Xu, P. K. Kanyingi, K. Wang, G. Li, B. Han, and X. Jiang, "Probabilistic small signal stability analysis with large scale integration of wind power considering dependence," *Renew. Sustain. Energy Rev.*, vol. 69, pp. 1258–1270, Mar. 2017.

[44] T. Zhou, Z. Chen, S. Bu, H. Tang, and Y. Liu, "Eigen-analysis considering time-delay and data-loss of WAMS and ITS application to WADC design based on damping torque analysis," *Energies*, vol. 11, no. 11, p. 3186, Nov. 2018.

[45] M. Amin and M. Molinas, "Small-signal stability assessment of power electronics based power systems: A discussion of impedance- and eigenvalue-based methods," *IEEE Trans. Ind. Appl.*, vol. 53, no. 5, pp. 5014–5030, Sep. 2017.

[46] S. Xia, S. Bu, X. Zhang, Y. Xu, B. Zhou, and J. Zhu, "Model reduction strategy of doubly-fed induction generator-based wind farms for power system small-signal rotor angle stability analysis," *Appl. Energy*, vol. 222, pp. 608–620, Jul. 2018.

[47] J. L. Domínguez-García, O. Gomis-Bellmunt, F. D. Bianchi, and A. Sumper, "Power oscillation damping supported by wind power: A review," *Renew. Sustain. Energy Rev.*, vol. 16, no. 7, pp. 4994–5006, Sep. 2012.

[48] R. Shah, N. Mithulananathan, and K. Y. Lee, "Design of robust power oscillation damping controller for large-scale PV plant," in *Proc. IEEE Power Energy Soc. Gen. Meeting*, San Diego, CA, USA, Jul. 2012, pp. 1–8.

[49] M. Wu, L. Xie, L. Cheng, and R. Sun, "A study on the impact of wind farm spatial distribution on power system sub-synchronous oscillations," *IEEE Trans. Power Syst.*, vol. 31, no. 3, pp. 2154–2162, May 2016.

[50] A. M. Vural, "Contribution of high voltage direct current transmission systems to inter-area oscillation damping: A review," *Renew. Sustain. Energy Rev.*, vol. 57, pp. 892–915, May 2016.

[51] H. Hasanvand, M. R. Arvan, B. Mozafari, and T. Amraee, "Coordinated design of PSS and TCSC to mitigate interarea oscillations," *Int. J. Elect. Power Energy Syst.*, vol. 78, pp. 194–206, Jun. 2016.

[52] Y. Yang, J. Zhao, H. Liu, Z. Qin, J. Deng, and J. Qi, "A matrix-perturbation-theory-based optimal strategy for small-signal stability analysis of large-scale power grid," *Protection Control Mod. Power Syst.*, vol. 3, no. 1, p. 34, 2018.

[53] S. Bu, X. Zhang, S. Xia, Y. Xu, B. Zhou, and X. Lu, "Reducing model complexity of DFIG-based wind turbines to improve the efficiency of power system stability analysis," *Energy Procedia*, vol. 142, pp. 971–976, Dec. 2017.

[54] C. Chen, W. Du, H. Wang, and T. Littler, "Sub-synchronous oscillations in power systems caused by grid-connected wind farms-a survey of mechanism studies," *CSEE J. Power Energy Syst.*, vol. 4, no. 4, pp. 495–503, Dec. 2018.

[55] J. Sun, M. Li, Z. Zhang, T. Xu, J. He, H. Wang, and G. Li, "Renewable energy transmission by HVDC across the continent: System challenges and opportunities," *CSEE J. Power Energy Syst.*, vol. 3, no. 4, pp. 353–364, Dec. 2017.

[56] W. Ren and E. Larsen, "A refined frequency scan approach to subsynchronous control interaction (SSCI) study of wind farms," *IEEE Trans. Power Syst.*, vol. 31, no. 5, pp. 3904–3912, Sep. 2016.

[57] M. Amin and M. Molinas, "A gray-box method for stability and controller parameter estimation in HVDC-connected wind farms based on nonparametric impedance," *IEEE Trans. Ind. Electron.*, vol. 66, no. 3, pp. 1872–1882, Mar. 2019.

[58] L. He and C.-C. Liu, "Parameter identification with PMUs for instability detection in power systems with HVDC integrated offshore wind energy," *IEEE Trans. Power Syst.*, vol. 29, no. 2, pp. 775–784, Mar. 2014.

[59] M. Cheah-Mane, L. Sainz, J. Liang, N. Jenkins, and C. E. Ugalde-Loo, "Criterion for the electrical resonance stability of offshore wind power plants connected through HVDC links," *IEEE Trans. Power Syst.*, vol. 32, no. 6, pp. 4579–4589, Nov. 2017.

[60] L. Huang, H. Xin, Z. Wang, K. Wu, H. Wang, and J. Hu, "A virtual synchronous control for voltage-source converters utilizing dynamics of DC-link capacitor to realize self-synchronization," *IEEE J. Emerg. Sel. Topics Power Electron.*, vol. 5, no. 4, pp. 1565–1577, Dec. 2017.

[61] L. Wang, J. Peng, Y. You, and H. Ma, "Iterative approach to impedance model for small-signal stability analysis," *IET Renew. Power Gener.*, vol. 13, no. 1, pp. 78–85, Jan. 2019.

[62] H. Liu, X. Xie, C. Zhang, Y. Li, and H. Liu, "Quantitative SSR analysis of series-compensated DFIG-based wind farms using aggregated RLC circuit model," *IEEE Trans. Power Syst.*, vol. 32, no. 1, pp. 474–483, Jan. 2017.

[63] H. Liu, X. Xie, and W. Liu, "An oscillatory stability criterion based on the unified DQ-frame impedance network model for power systems with high-penetration renewables," *IEEE Trans. Power Syst.*, vol. 33, no. 3, pp. 3472–3485, May 2018.

[64] H. Liu, X. Xie, J. He, T. Xu, Z. Yu, C. Wang, and C. Zhang, "Subsynchronous interaction between direct-drive PMSG based wind farms and weak AC networks," *IEEE Trans. Power Syst.*, vol. 32, no. 6, pp. 4708–4720, Nov. 2017.

[65] H. Liu, X. Xie, X. Gao, H. Liu, and Y. Li, "Stability analysis of SSR in multiple wind farms connected to series-compensated systems using impedance network model," *IEEE Trans. Power Syst.*, vol. 33, no. 3, pp. 3118–3128, May 2018.

[66] L. Piyasinghe, Z. Miao, J. Khazaei, and L. Fan, "Impedance model-based SSR analysis for TCSC compensated type-3 wind energy delivery systems," *IEEE Trans. Sustain. Energy*, vol. 6, no. 1, pp. 179–187, Jan. 2015.

[67] S. Bu, X. Zhang, J. Zhu, and X. Liu, "Comparison analysis on damping mechanisms of power systems with induction generator based wind power generation," *Int. J. Elect. Power Energy Syst.*, vol. 97, pp. 250–261, Apr. 2018.

[68] D. N. Hussein, M. Matar, and R. Iravani, "A wideband equivalent model of type-3 wind power plants for EMT studies," *IEEE Trans. Power Del.*, vol. 31, no. 5, pp. 2322–2331, Oct. 2016.

[69] L. Wang, X. Xie, Q. Jiang, H. Liu, Y. Li, and H. Liu, "Investigation of SSR in practical DFIG-based wind farms connected to a series-compensated power system," *IEEE Trans. Power Syst.*, vol. 30, no. 5, pp. 2772–2779, Sep. 2015.

[70] Z. Miao, "Impedance-model-based SSR analysis for type 3 wind generator and series-compensated network," *IEEE Trans. Energy Convers.*, vol. 27, no. 4, pp. 984–991, Dec. 2012.

[71] L. Fan and Z. Miao, "Nyquist-stability-criterion-based SSR explanation for type-3 wind generators," *IEEE Trans. Energy Convers.*, vol. 27, no. 3, pp. 807–809, Sep. 2012.

[72] E. V. Larsen, "Wind generators and series-compensated AC transmission lines," in *Proc. IEEE Power Energy Soc. Gen. Meeting*, San Diego, CA, USA, Jul. 2012, pp. 1–4.
[73] H. Ma, P. Brogan, K. Jensen, and R. Nelson, "Sub-synchronous control interaction studies between full-converter wind turbines and series-compensated AC transmission lines," in *Proc. IEEE Power Energy Soc. General Meeting*, San Diego, CA, USA, Jul. 2012, pp. 1–5.
[74] S. Q. Bu, W. Du, and H. F. Wang, "Investigation on probabilistic small-signal stability of power systems as affected by offshore wind generation," *IEEE Trans. Power Syst.*, vol. 30, no. 5, pp. 2479–2486, Sep. 2015.
[75] M. Amin and M. Molinas, "Impedance based stability analysis of VSC-based HVDC system," in *Proc. IEEE Eindhoven PowerTech*, Eindhoven, The Netherlands, Jul. 2015, pp. 1–6.
[76] L. Xu, L. Fan, and Z. Miao, "DC impedance-model-based resonance analysis of a VSC-HVDC system," *IEEE Trans. Power Del.*, vol. 30, no. 3, pp. 1221–1230, Jun. 2015.
[77] H. Liu and J. Sun, "Impedance-based stability analysis of VSC-based HVDC systems," in *Proc. IEEE 14th Workshop Control Model. Power Electron. (COMPEL)*, Salt Lake City, UT, USA, Jul. 2013, pp. 1–8.
[78] M. Amin, A. Rygg, and M. Molinas, "Impedance-based and eigenvalue based stability assessment compared in VSC-HVDC system," in *Proc. IEEE Energy Convers. Congr. Expo. (ECCE)*, Milwaukee, WI, USA, Sep. 2016, pp. 1–8.
[79] L. Xu and L. Fan, "Impedance-based resonance analysis in a VSC-HVDC system," *IEEE Trans. Power Del.*, vol. 28, no. 4, pp. 2209–2216, Oct. 2013.
[80] J. Lyu, X. Cai, and M. Molinas, "Frequency domain stability analysis of MMC-based HVdc for wind farm integration," *IEEE J. Emerg. Sel. Topics Power Electron.*, vol. 4, no. 1, pp. 141–151, Mar. 2016.
[81] J. Lyu, X. Cai, and M. Molinas, "Optimal design of controller parameters for improving the stability of MMC-HVDC for wind farm integration," *IEEE J. Emerg. Sel. Topics Power Electron.*, vol. 6, no. 1, pp. 40–53, Mar. 2018.
[82] J. Sun and H. Liu, "Sequence impedance modeling of modular multilevel converters," *IEEE J. Emerg. Sel. Topics Power Electron.*, vol. 5, no. 4, pp. 1427–1443, Dec. 2017.
[83] D. Shu, V. Dinavahi, X. Xie, and Q. Jiang, "Shifted frequency modeling of hybrid modular multilevel converters for simulation of MTDC grid," *IEEE Trans. Power Del.*, vol. 33, no. 3, pp. 1288–1298, Jun. 2018.
[84] C. Zou, H. Rao, S. Xu, Y. Li, W. Li, Jun Chen, X. Zhao, Y. Yang, and B. Lei, "Analysis of resonance between a VSC-HVDC Converter and the AC Grid," in *Proc. IEEE Trans. Power Electron.*, vol. 33, no. 12, pp. 10157–10168, Dec. 2018.
[85] M. Cespedes and J. Sun, "Impedance modeling and analysis of grid-connected voltage-source converters," *IEEE Trans. Power Electron.*, vol. 29, no. 3, pp. 1254–1261, Mar. 2014.
[86] B. Wen, D. Boroyevich, R. Burgos, P. Mattavelli, and Z. Shen, "Analysis of *dq* small-signal impedance of grid-tied inverters," *IEEE Trans. Power Electron.*, vol. 31, no. 1, pp. 675–687, Jan. 2016.
[87] A. Rygg, M. Molinas, C. Zhang, and X. Cai, "A modified sequence-domain impedance definition and its equivalence to the dq-domain impedance definition for the stability analysis of AC power electronic systems," *IEEE J. Emerg. Sel. Topics Power Electron.*, vol. 4, no. 4, pp. 1383–1396, Dec. 2016.
[88] S. Shah and L. Parsa, "Impedance modeling of three-phase voltage source converters in DQ, sequence, and phasor domains," *IEEE Trans. Energy Convers.*, vol. 32, no. 3, pp. 1139–1150, Sep. 2017.
[89] H. Liu and J. Sun, "Voltage stability and control of offshore wind farms with AC collection and HVDC transmission," *IEEE J. Emerg. Sel. Topics Power Electron.*, vol. 2, no. 4, pp. 1181–1189, Dec. 2014.
[90] D. Shu, X. Xie, H. Rao, X. Gao, Q. Jiang, and Y. Huang, "Sub-and super-synchronous interactions between STATCOMs and weak AC/DC transmissions with series compensations," *IEEE Trans. Power Electron.*, vol. 33, no. 9, pp. 7424–7437, Sep. 2018.
[91] H. Xin, Z. Li, W. Dong, L. Zhang, Z. Wang, and J. Zhao, "Generalized-impedance and stability criterion for grid-connected converters," 2017, *arXiv:1706.05625*. [Online]. Available: https://arxiv.org/abs/1706.05625
[92] A. Rygg, M. Molinas, E. Unamuno, C. Zhang, and X. Cai, "A simple method for shifting local dq impedance models to a global reference frame for stability analysis," 2017, *arXiv:1706.08313*. [Online]. Available: https://arxiv.org/abs/1706.08313
[93] Y. Wang, X. Wang, Z. Chen, and F. Blaabjerg, "Small-signal stability analysis of inverter-fed power systems using component connection method," *IEEE Trans. Smart Grid*, vol. 9, no. 5, pp. 5301–5310, Sep. 2018.
[94] J. Sun, "Small-signal methods for AC distributed power systems—A review," *IEEE Trans. Power Electron.*, vol. 24, no. 11, pp. 2545–2554, Nov. 2009.
[95] X. Wang, L. Harnefors, and F. Blaabjerg, "Unified impedance model of grid-connected voltage-source converters," *IEEE Trans. Power Electron.*, vol. 33, no. 2, pp. 1775–1787, Feb. 2018.
[96] B. Wen, R. Burgos, D. Boroyevich, P. Mattavelli, and Z. Shen, "AC stability analysis and *dq* frame impedance specifications in power-electronics-based distributed power systems," *IEEE J. Emerg. Sel. Topics Power Electron.*, vol. 5, no. 4, pp. 1455–1465, Dec. 2017.
[97] J. Sun, "Impedance-based stability criterion for grid-connected inverters," *IEEE Trans. Power Electron.*, vol. 26, no. 11, pp. 3075–3078, Nov. 2011.
[98] W. Wu, L. Zhou, Y. Chen, A. Luo, Y. Dong, X. Zhou, Q. Xu, L. Yang, and J. M. Guerrero, "Sequence-impedance-based stability comparison between VSGs and traditional grid-connected inverters," *IEEE Trans. Power Electron.*, vol. 34, no. 1, pp. 46–52, Jan. 2019.
[99] J. Gao, J. Zhao, K. Qu, and F. Li, "Reconstruction of impedance-based stability criterion in weak grid," in *Proc. 3rd Int. Conf. Intell. Green Building Smart Grid (IGBSG)*, Yi-Lan, Taiwan, Apr. 2018, pp. 1–4.
[100] H. Liu and X. Xie, "Impedance network modeling and quantitative stability analysis of sub-/super-synchronous oscillations for large-scale wind power systems," *IEEE Access*, vol. 6, pp. 34431–34438, Jun. 2018.
[101] C. Zhang, X. Cai, A. Rygg, and M. Molinas, "Sequence domain SISO equivalent models of a grid-tied voltage source converter system for small-signal stability analysis," *IEEE Trans. Energy Convers.*, vol. 33, no. 2, pp. 741–749, Jun. 2018.
[102] A. Rygg, M. Molinas, C. Zhang, and X. Cai, "On the equivalence and impact on stability of impedance modeling of power electronic converters in different domains," *IEEE J. Emerg. Sel. Topics Power Electron.*, vol. 5, no. 4, pp. 1444–1454, Dec. 2017.
[103] W. Chen, X. Xie, D. Wang, H. Liu, and H. Liu, "Probabilistic stability analysis of subsynchronous resonance for series-compensated DFIG-based wind farms," *IEEE Trans. Sustain. Energy*, vol. 9, no. 1, pp. 400–409, Jan. 2018.
[104] K. N. Hasan, R. Preece, and J. V. Milanović, "Existing approaches and trends in uncertainty modelling and probabilistic stability analysis of power systems with renewable generation," *Renew. Sustain. Energy Rev.*, vol. 101, pp. 168–180, Mar. 2019.
[105] S. Bu, W. Du, H. Wang, Z. Chen, L. Xiao, and H. Li, "Probabilistic analysis of small-signal stability of large-scale power systems as affected by penetration of wind generation," *IEEE Trans. Power Syst.*, vol. 27, no. 2, pp. 762–770, May 2012.
[106] S. Bu, W. Du, and H. Wang, "Probabilistic analysis of small-signal rotor angle/voltage stability of large-scale AC/DC power systems as affected by grid-connected offshore wind generation," *IEEE Trans. Power Syst.*, vol. 28, no. 4, pp. 3712–3719, Nov. 2013.

YONG HU received the B.Eng. degree in electrical engineering and automation from the Agricultural University of Hebei, Baoding, Hebei, China, in 2014, and the M.Eng. degree in electrical engineering from Beijing Jiaotong University, Beijing, China, in 2017. He is currently pursuing the Ph.D. degree with the Department of Electrical Engineering, The Hong Kong Polytechnic University, Hong Kong.

His current research interests include stability analysis of power systems with renewable energy integration, optimal strategies to improve power system stability, and optimal planning as well as operation of power systems with renewable energy generations and electric vehicles.

SIQI BU (S'11–M'12–SM'17) received the Ph.D. degree in electric power and energy research cluster from the Queen's University of Belfast, Belfast, U.K., in 2012, where he continued his postdoctoral research work before entering industry.

He was with National Grid U.K. as an Experienced U.K. National Transmission System Planner and Operator. He is currently an Assistant Professor with The Hong Kong Polytechnic University, Hong Kong, and a Chartered Engineer with the U.K. Royal Engineering Council, London, U.K. His research interests include power system stability analysis and operation control, including wind power generation, PEV, HVDC, FACTS, ESS, and VSG. He received various prizes due to excellent performances and outstanding contributions in operational and commissioning projects during the employment with the National Grid U.K. He was a recipient of the Outstanding Reviewer Awards from the IEEE TRANSACTIONS ON SUSTAINABLE ENERGY, the IEEE TRANSACTIONS ON POWER SYSTEMS, *Applied Energy*, *Renewable Energy*, and *International Journal of Electrical Power & Energy Systems*. He is also an Associate Editor of IEEE ACCESS and *CSEE Journal of Power and Energy Systems*, a Guest Editor of the *IET Renewable Power Generation* and *Energies*, and an Editor of the *Protection and Control of Modern Power Systems*.

BIN ZHOU (S'11–M'13–SM'17) received the B.Sc. degree in electrical engineering from Zhengzhou University, Zhengzhou, China, in 2006, the M.S. degree in electrical engineering from the South China University of Technology, Guangzhou, China, in 2009, and the Ph.D. degree from The Hong Kong Polytechnic University, Hong Kong, in 2013. He was a Research Associate and a Postdoctoral Fellow with the Department of Electrical Engineering, The Hong Kong Polytechnic University. He is currently an Associate Professor with the College of Electrical and Information Engineering, Hunan University, Changsha, China. His research interests include smart grid operation and planning, renewable energy generation, and energy efficiency.

YI LIU received the B.S. degree in electrical engineering from Tianjin University, Tianjin, China, in 2008, and the Ph.D. degree from the Institute of Electrical Engineering, Chinese Academy of Sciences, China, in 2015.

He is currently with the Institute of Electrical Engineering, Chinese Academy of Sciences, China. His research interests include power system economics and stability, including wind energy, energy storage, and HVDC technology.

CHENG-WEI FEI received the B.S. degree in electrical engineering and automation from the Fujian University of Technology, Fuzhou, China, in 2007, the M.S. degree in aerospace engineering from Shenyang Aerospace University, Shenyang, China, in 2010, and the Ph.D. degree in aerospace engineering from Beihang University, Beijing, China, in 2014.

From 2014 to 2017, he was a Postdoctoral Fellow (Hong Kong Scholars) with the Department of Mechanical Engineering, The Hong Kong Polytechnic University, Hong Kong, and then from 2017 to 2018, he was a Research Fellow with the Department of Mechanical and Aerospace Engineering, The Hong Kong University of Science and Technology, Hong Kong. Since 2018, he has been a Research Professor with the Department of Aeronautics and Astronautics, Fudan University, Shanghai, China. He is the author of one book, more than 100 articles, and three inventions. His research interests include surrogate model, multidisciplinary design optimization (MDO), reliability-based design optimization (RBDO), and structural health monitoring with machine/deep learning for aircrafts and aero-engines.

Dr. Fei is also a member of the American Institute of Aeronautics and Astronautics (AIAA), the Chinese Society of Aeronautics and Astronautics (CSAA), and the American Society of Mechanical Engineers (ASME). He was a recipient of the National Excellent Doctoral Dissertation, in 2016, the Hong Kong Scholars Awards, in 2016, The Academic Scholarship of Chinese Ministry of Education for Ph.D. candidates, in 2012, and the National Graduate Scholarship of China, in 2012. He is also the Lead Guest Editor of *Advances in Acoustics and Vibration* and *Advances in Mechanical Engineering*. He is also a Reviewer of more than ten journals, such as IEEE ACCESS, *Nonlinear Dynamics*, *Mechanical Systems and Signal Processing*, *Aerospace Science and Technology*, *Aerospace Science and Technology*, *Reliability Engineering & System Safety*, and so on.